Identification of BeO and BeOxDy in melted zones of the JET Be limiter tiles: Raman study using comparison with laboratory samples

Nuclear Materials and Energy 17 (2018) 295–301

Contents lists available at ScienceDirect

Nuclear Materials and Energy

journal homepage: www.elsevier.com/locate/nme

Identification of BeO and BeOxDy in melted zones of the JET Be limiter tiles: Raman study using comparison with laboratory samples

M. Kumar[a], C. Makepeace[b,f], C. Pardanaud[a,*], Y. Ferro[a], E. Hodille[a], C. Martin[a], P. Roubin[a], A. Widdowson[b], T. Dittmar[c], C.h. Linsmeier[c], C.P. Lungu[d], C. Porosnicu[d], I. Jepu[b,d], P. Dinca[d], M. Lungu[d], O.G. Pompilian[d], JET contributors[e,**]

[a] Aix Marseille Univ, CNRS, PIIM, Marseille, France
[b] Department of Materials, University of Oxford, Parks Road, Oxford OX1 3PH, UK
[c] Forschungszentrum Jülich GmbH, Institut für Energie- und Klimaforschung - Plasmaphysik, Jülich 52425, Germany
[d] National Institute for Laser, Plasma and Radiation Physics, Magurele-Bucharest 077125, Romania
[e] EUROfusion Consortium, JET, Culham Science Centre, Abingdon OX14 3DB, UK
[f] Culham Centre for Fusion Energy, Culham Science Centre, Abingdon, OX14 3DB, UK

ARTICLE INFO

Keywords:
Beryllium oxide
Beryllium deuteroxide
D trapping
Melting

ABSTRACT

Beryllium oxide (BeO) and deuteroxide (BeO_xD_y) have been found on the melted zone of a beryllium tile extracted from the upper dump plate of JET-ILW (2011–2012 campaign). Results have been obtained using Raman microscopy, which is sensitive to both the chemical bond and crystal structure, with a micrometric lateral resolution. BeO is found with a wurtzite crystal structure. BeO_xD_y is found as three different types which are not the β-phase but behaves as molecular species like $Be(OD)_2$, $O(Be\text{-}D)_2$ and DBeOD. The presence of a small amount of trapped D_2O is also suspected. Our results therefore strongly suggest that D trapping occurs after melting through the formation of deuteroxides. The temperature increase favors the formation of crystal BeO which favors deuterium trapping through OD bonding.

1. Introduction

Plasma facing components (PFCs) are first wall made of tungsten and/or beryllium in nowadays tokamaks and experience plasma-wall interactions [1], such as in the JET tokamak which is equipped with a ITER-like wall (ILW), since 2011 [2]. There, the PFCs are subject to high heat loads and ion irradiation that modify material physical properties, particularly in leading to erosion and deposition processes [3]. Predicting these modifications is of concern for long time operation and safety issues [4]. Some key points under study are: the migration of eroded elements in the tokamak [5,6], the melting of PFC materials [7,8], the production of dust [9–11], the hydrogen isotope retention [12,13], the formation of oxides because of the presence of both impurity and hot surfaces [14], and finally the presence of hydrogen inside oxides [15], with hydroxides formation hypothesized [16].

The Raman microscopy technique is sensitive to the near surface (few tens of nanometers) with a micrometric lateral resolution. It probes atomic vibrations, being thus able to distinguish chemical bonds, and has been used in the fusion community for many years, especially for carbon material studies [17]. In a series of recent works, we have benchmarked this technique for beryllium materials on laboratory synthetized samples in order to use it for the post-mortem analysis of JET samples [18–20].

We report here on the specific Raman analysis of two tiles which occupied the same place on the JET upper dump plate, but in two different campaigns, one which led to melting zones and a second one without melting zones and we focus on oxide and hydrogen behaviors. This comparative work is complementary to a wider work that includes other post-mortem analyses on these two tiles and that deals with the effect of beryllium oxide on retention in JET-ILW. The paper is organized as follows. Details on the tiles and the campaigns are given together with the Raman technique in Section 2. Results are given in Section 3 and are discussed in Section 4. Finally, a conclusion is given in Section 5.

2. Experimental section

A first tile, situated in the upper dump plate of JET-ILW was

* Corresponding author.
E-mail address: cedric.pardanaud@univ-amu.fr (C. Pardanaud).
** See the author list of "X. Litaudon et al 2017 Nucl. Fusion 57 102001.

https://doi.org/10.1016/j.nme.2018.11.008
Received 29 July 2018; Received in revised form 9 November 2018; Accepted 10 November 2018
Available online 06 December 2018

extracted in 2012 from the limiter, after the 2011–2012 campaign. The plasma of that campaign was composed of 6 h of limiter phase and 13 h of divertor phase, with an input energy per tile of 150 GJ [21]. This tile will be referred as "2011–2012 campaign tile" in the following document. A second tile, situated in the same location as the first, was extracted in 2014, from the limiter, after the 2013–2014 campaign. The plasma of that campaign was composed of 5.2 h of limiter phase and 14.2 h of divertor phase, with an input energy per tile of 201 GJ. This tile will be referred as "2013–2014 campaign tile" in the following document. Both tiles were analyzed in between the end of 2017 and the beginning of 2018 by means of Raman microscopy.

A codeposit laboratory sample was produced in the facilities of the National Institute for Laser, Plasma and Radiation Physics (NILPRP) in Romania, using thermionic vacuum (TVA), [22]. Be,O and C were deposited in a D_2 atmosphere, to mimick the composition of deposits found on JET divertor tile 1 [23].

Raman spectra were recorded in back-scattering geometry in a Raman mapping mode using a Horiba-Jobin-Yvon HR LabRAM HR800 apparatus (with × 100 objective, with a numerical aperture of 0.9 and sometimes × 50 objective with a numerical aperture of 0.5 for mappings, both with λ_L = 514.5 nm). The laser power was kept at ~ 1 mW μm^{-2} to prevent any damage. The grating used (600 lines/mm) leads to a spectral resolution of 1 cm^{-1}. The lateral definition of the maps was most of the time chosen to be few microns, except for a zone which was investigated in deeper details, with 0.5 µm.

3. Results

Raman spectroscopy was performed on many locations of an upper dump plate extracted from the 2011–2012 and 2013–2014 campaigns. The signal was found to be heterogeneous and Fig. 1 is obtained by averaging on a ≈ 1000 μm^2 zone. This figure therefore displays the comparison between typical averaged Raman spectra of these two upper dump plate tiles and those of some reference samples: defective Be, beryllium deuteride, oxide and carbide. These two latter components could in principle be found in the walls as oxygen and carbon are major pollutants. We first describe the Raman spectroscopy of the reference samples (bullets) and then we make first conclusions for JET samples.

- Crystalline Be spectrum displays a unique Raman active mode close to 455 cm^{-1}. Introducing defects gives rise to two groups of bands called PDOS and 2PDOS (PDOS stands for phonon density of states), with an empty spectral region between these two groups from 650 to 750 cm^{-1}. These PDOS bands were never found to exceed 25% of the height of the 455 cm^{-1} band. More details on the Be band can be found in [18], and later on, in Fig. 4.
- Crystalline Be deuteride (BeD_2) can exist under several forms [24], and we display here the α phase spectrum, extracted from [20]. Modes are distributed from 250 to 1000 cm^{-1}, then there is a gap from 1000 to 1400 cm^{-1} and again modes from 1400–1550 cm^{-1} (see [20] for the higher frequency modes at 1700 cm^{-1}). The main difference with the other reported deuteride phases, according to calculations, is that, for the other phases, only the low-lying frequency modes exist and there is no vibrational modes at a frequency higher than 1240 cm^{-1}. Then, the presence of bands falling in the 1400–1550 cm^{-1} spectral region are a strong indicator of the presence of α-BeD_2 phase. In Fig. 1, the stars correspond to values found in [25] for α-BeH_2, modified to take account of the isotopic shift (modification is done by ~~using~~ multiplying by a scaling factor that takes into account the ratio of the reduced masses of the Be-H and Be-D vibrators,).
- Crystalline Be oxide (BeO) can exist in different phases [26], but the most stable is the wurtzite [27] (and references therein). Its spectrum is mainly composed of a strong band at ≈ 680 cm^{-1}, a medium band at 723 cm^{-1} and two weak bands at 337 and 1088 cm^{-1} [28]. Recent calculations have predicted the existence of a BeO_2 phase (beryllium peroxide) [29], with vibrational modes falling in the range 480–530 and 680–850 cm^{-1}, plus another degenerate mode at 1125 cm^{-1}.
- The first Raman spectra of amorphous beryllium carbide were obtained in [18]. Bands fall in the range 500–1000 cm^{-1}. Be_2C was found to coexist with amorphous carbon, whose bands fall in the range 1000–1600 cm^{-1}. Note that hydrogenated amorphous carbon can also give rise to a linear background with a positive slope [30] (and references therein). Linear backgrounds when dealing with carbon materials are most of the time due to some photoluminescence mechanism involving hydrogen atoms in competition with the Raman mechanism.

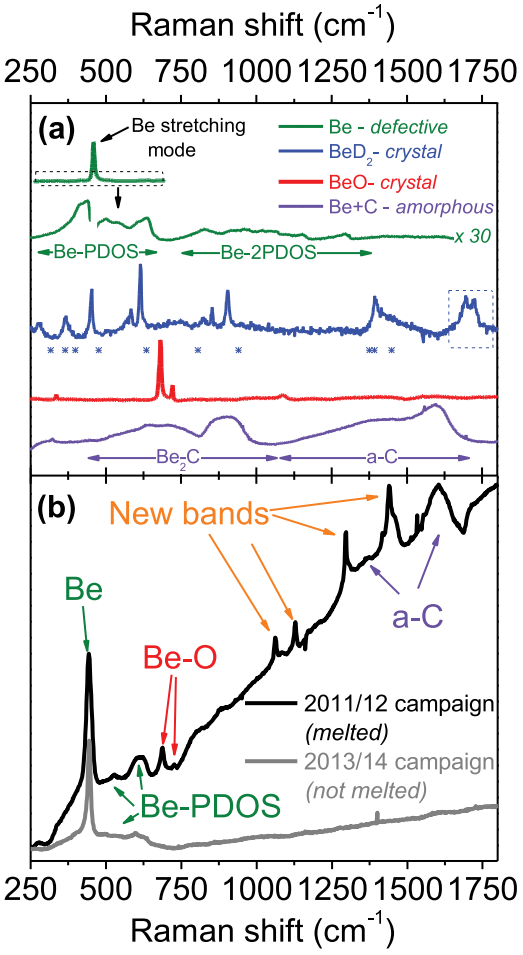

Fig. 1. Comparison of reference sample and JET-ILW sample Raman spectra. (a) Raman spectra from reference samples are defective beryllium (extracted from [18]), beryllium deuteride (extracted from [20]), beryllium oxide and beryllium carbide (extracted from [18]). Stars are from beryllium hydrides data [25] isotopically shifted for the purpose. (b) Raman spectra from two JET samples: 2011–2012 and 2013–2014 campaign tiles.

The 2011–2012 and 2013–2014 campaign tile spectra display the crystalline Be band and they also display the PDOS and 2PDOS bands: this shows that both samples correspond to defective crystalline Be. Spectra display a positive slope which is much higher in the case of the 2011–2012 campaign tile than in the case of the 2013–2014 campaign tile. As mentioned previously, this slope can be associated to the presence of hydrogenated amorphous carbon that is thus most probably present in the 2011–2012 campaign tile while it is less clear for the 2013–2014 campaign tile. Beryllium oxide under the wurtzite form is detected only in the 2011–2012 campaign tile. Again, in the case of the

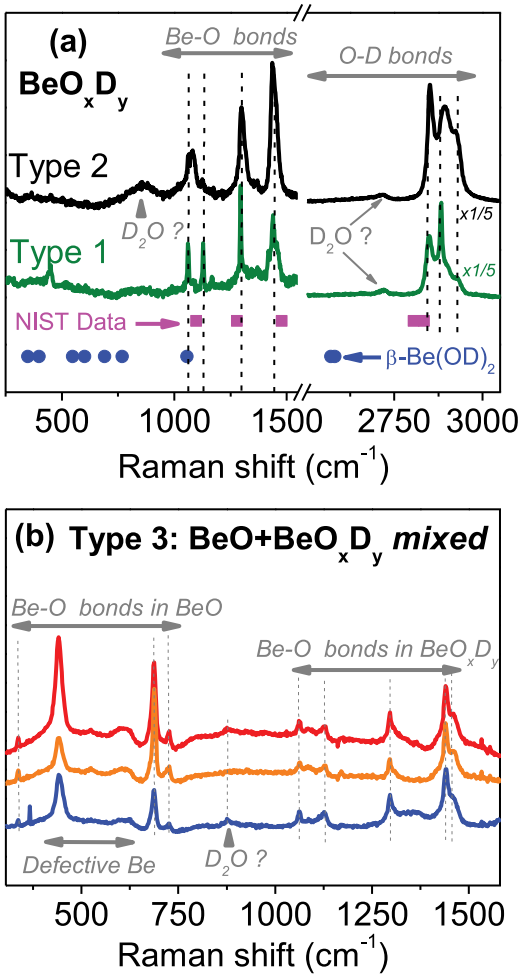

Fig. 2. Raman spectra of the 2011–2012 campaign tile in various zones. (a) Identification of Type 1 and Type 2 deuteroxides. The intensity corresponding to the 2700–3000 cm^{-1} spectral range has been divided by 5. Blue points are from [31] and magenta points are from [32] (b) Identification of Type 3 deuteroxide, coexisting with the oxide. A background due to carbon contamination was removed in (a) and (b). (For interpretation of the references to colour in this figure legend, the reader is referred to the web version of this article.)

2011–2012 campaign tile only, four strong new bands, lying at 1062 1129, 1296 and 1440 cm^{-1}, are detected. Instinctively, one think to attribute these bands to the presence of beryllium deuteride phase. Even if the 1440 cm^{-1} band falls in the 1400–1500 cm^{-1} spectral region corresponding to the α-BeD_2 phase, and could in a first look be attributed to a beryllium deuterated phase, this hypothesis is ruled out because:

- the three other bands fall in the 1000–1400 cm^{-1} spectral region, where there is no band related to beryllium deuteride phase,
- there are no bands at low frequencies, whereas there should be present for beryllium deuteride phase.

This is then not possible to attribute the bands at 1062 1129, 1296 and 1440 cm^{-1} to beryllium deuteride phase. The question of the origin of these new bands remains open.

Another candidate to explain these four bands in the 2011–2012 campaign tile is beryllium deuteroxide. However, the phase diagram of such material is still lacking. Nevertheless, whatever the deuteroxide phase is, there should exist some O—D bond signals that generally falls in the range 2200–2800 cm^{-1}. Fig. 2a displays Raman spectra from two different spots of the 2011–2012 campaign tile which are spectrally extended up to 3000 cm^{-1}. Contrary to Fig. 1 for which data were averaged on a large zone, these spectra correspond to homogenous responses of the sample (spot size of typically a few μm^2) and two types (named Type 1 and Type 2) have been identified here. For these two types, three very intense overlapping bands at 2850, 2885 and 2928 cm^{-1} together with a weak asymmetric band at 2720 cm^{-1} are measured. These band positions are consistent with the presence of O—D bonds. Raman spectra of the most documented deuteroxide phase (the β-$Be(OD)_2$ phase, called behoite) is composed of weak bands at 349, 400, 549, 602, 690 and 769 cm^{-1} together with more intense bands at 1056, 2570 and 2582 cm^{-1} [31]. As there is no agreement between the frequencies of the JET sample spectrum and those of the β-$Be(OD)_2$ reference spectrum, we conclude that the deuteroxide detected in JET is not the behoite phase. The other reference materials we found in the literature are also displayed in the NIST webbook chemistry database and comes from [32]. Be—O bonds were found at 1098, 1279, and 1477 cm^{-1}, Be—D bonds were found at 1643 and 1663 cm^{-1}, and O—D bonds were found at 2805 and 2834 cm^{-1}. There is a good agreement between the bands displayed in Fig. 2a for the JET samples (Type 1 and Type 2) and for these NIST data. The bands at 1643 and 1663 cm^{-1} are not observed in JET samples, but it could be explained because the technique used in [32] is infrared spectroscopy, which can change the intensities according to quantum selection rules. It can also be due to the underlying broad band due to hydrogenated amorphous carbon which peaks at 1600 cm^{-1} and which can hinder the Be—D band detection, as these bands are broad (typically ≈ 100 cm^{-1}) and not well-defined. We thus conclude that these Type 1 and Type 2 spectra most probably correspond to deuteroxides.

Type 1, 2, 3 spectra displayed in Fig. 2 are representative of the three distinct physico-chemical environments found in this investigation. Type 1 and 2 can be observed with or without the presence of Be or wurtzite BeO bands while Type 3 (Fig. 2b) exists only when wurtzite BeO bands (at 680 and 723 cm^{-1}) are present. Type 1 and 2 spectra only slightly differ. As for band widths, they are smaller for Type 1 than for Type 2 bands (typically 7 cm^{-1} and 30 cm^{-1}, respectively), suggesting a more organized environment in the case of Type 1 than in the case of Type 2. As for band positions:

- at ~ 1100 cm^{-1}, there is a doublet for Type 1 (1060 and 1127 cm^{-1}) and a singlet for Type 2 (1077 cm^{-1})
- at ~ 1440 cm^{-1}, there is an overlapping triplet for Type 1 (1420, 1437 and 1454 cm^{-1}) and a singlet for Type 2 (1438 cm^{-1})
- two weak bands are observed at 1167 and 1368 cm^{-1} for Type 1 and only the latter is observed for Type 2
- the bands at 1295 cm^{-1} and 2882 cm^{-1} for Type 1 are upshifted at 1299 cm^{-1} and 2893 cm^{-1} for Type 2, respectively
- there is a broad band at 855 cm^{-1} which is more intense for Type 2 than for Type 1

As for the intensities of the main bands in the Be—O (O—D) region, the intensity at 1295 (2882) cm^{-1} is larger than that at 1437 (2848) cm^{-1} for Type 1 (I_{1295}/I_{1437} is ~ 1.35) while it is the contrary for Type 2 (I_{1295}/I_{1437} is ~ 0.71). The relative ratios I_{2882}/I_{1295} and I_{2848}/I_{1437} stay roughly uniform over the sample zone investigated, meaning that they correspond to the same species. Therefore, even though Type 1 and Type 2 are probably not composed with a single deuteroxide species, we can characterize Type 1 and Type 2 with these two main couples of bands, (1295 and 2882 cm^{-1}) and (1437 and 2848 cm^{-1}), respectively.

Type 3 spectra are very similar to those of Type 1 (see Fig. 2b when three examples of Type 3 spectra are displayed, and a Type 1 spectrum is reported from Fig. 2a in green). The two bands at 680 and 723 cm^{-1} from the wurtzite BeO are always observed in the case of Type 3 spectra, with various relative intensities, the lowest value of I_{723}/I_{680} being ~ 0.35. We also report a weak and broad band at 878 cm^{-1} which origin could be similar to that at 855 cm^{-1} in the case of Type 1

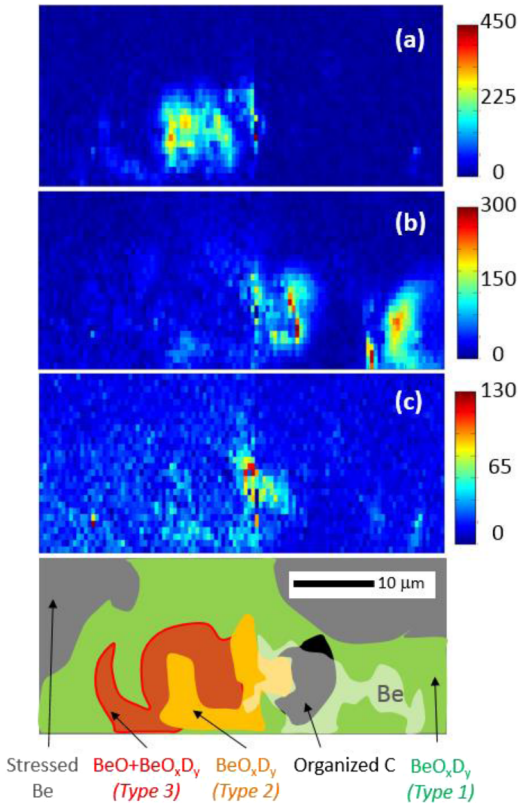

Fig. 3. Raman mapping of a zone of the 2011–2012 campaign tile. (a) BeO band intensity. (b) BeO_xD_y Type 1 band intensity. (c) BeO_xD_y Type 2 band intensity. (d) Spatial repartition of the different phases. This cartoon also takes into account other maps of the band positions and intensities (not displayed here). Note that amorphous carbon is found everywhere.

and 2. Remarkably, these three types of BeO_xD_y are found only in melted zones of the 2011–2012 campaign tile and not in the 2013–2014 campaign tile which was not melted, nor in the non-melted zones of the 2011–2012 campaign tile.

Maps of the intensities and frequencies of the most relevant Raman bands have been recorded for a melted zone of the 2011–2012 campaign tile and Fig. 3abc displays three of these maps while Fig. 3d displays a scheme of the spatial distribution of the various phases, Be, BeO, BeO_xD_y and C, that could be deduced from the ensemble of maps. The spatial distribution of BeO has been obtained by displaying the 680 cm^{-1} band intensity (Fig. 3a) which correlates very well with the frequency map (not shown). The spatial distribution of BeO_xD_y Type 1 and 2 have been obtained by displaying the 1295 and 855 cm^{-1} band intensities, (Fig. 3b and c, respectively). The corresponding frequency maps (not shown) correlates only partially, due to complex radiative transfer processes at play in heterogeneous media. The main points are listed below:

- two types of beryllium structures are found: stressed and not stressed. The band frequency of the stressed Be is ~ 10 cm^{-1} downshifted compared to normal Be.
- BeO was found at the lower middle part of the investigated zone, in a ≈ 10 µm nucleus
- BeO_xD_y Type 3 is found mixed with BeO
- BeO_xD_y Type 2 is found only close to BeO and interfacing with Type 1
- BeO_xD_y Type 1 is the main phase found in the zone, outside the Type 3 and Type 2 locations, and with the maximum intensity in the lower left corner of the zone (Fig. 3b).
- hydrogenated amorphous carbon is found everywhere (easily observed because of it high Raman cross-section)
- a zone of organized carbon is found at the left of the BeO nucleus

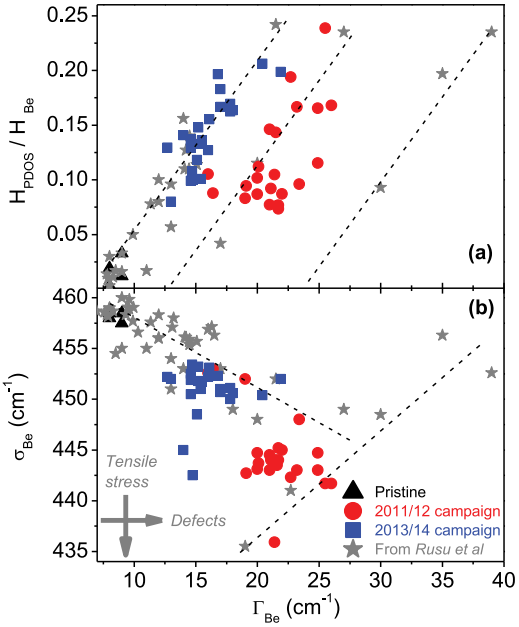

Fig. 4. Raman parameter plots characterizing the Be phase. (a) H_{PDOS}/H_{Be} as a function of Γ_{Be}. (b) σ_{Be} as a function of Γ_{Be}. Data in grey and black from [18] have been added for comparison. Lines are guides for the eyes. (For interpretation of the references to colour in this figure legend, the reader is referred to the web version of this article.)

This Raman map of the various phases suggests that BeO_xD_y Types 1, 2 and 3 are roughly concentrically distributed according to the nucleus containing BeO. More precisely, Type 3 is mixed in the BeO nucleus, Type 2 is found at the neighboring of the BeO nucleus whereas Type 1 is found elsewhere.

Fig. 4 focuses on the Be phases and displays spectroscopic parameters of the 455 cm^{-1} Be band for spectra recorded at various locations separated by millimeter distances on the 2011–2012 campaign tile (in red) and the 2013–2014 campaign tile (in blue). The spectroscopic parameters are the relative band height ratio formed with the PDOS related band height and the Be Raman active mode related band height: H_{PDOS}/H_{Be}, the band position related to the Be Raman active mode: σ_{Be}, and its full width at half maximum: Γ_{Be}. H_{PDOS}/H_{Be} (Fig. 4a) and σ_{Be} (Fig. 4b) are plotted in function of Γ_{Be}. It was shown that these parameters can be correlated and reflect the existence of defects and tensile stress in the material. Previous data from [18] obtained for various implanted and deposited mixed Be based samples synthesized in laboratory are displayed for comparison (in grey, see also Figure 7 of [18]). Crystalline Be corresponds to $H_{PDOS}/H_{Be} \approx 0$, $\sigma_{Be} \approx 457$ cm^{-1} and $\Gamma_{Be} \approx 9$ cm^{-1} while averaged parameters for the 2013–2014 campaign tile (the 2011–2012 campaign tile) are $H_{PDOS}/H_{Be} \approx 0.14$ (0.16), $\sigma_{Be} \approx 451$ (445) cm^{-1} and $\Gamma_{Be} \approx 16$ (22) cm^{-1}. Fig. 4 shows that data from both JET and laboratory samples are not randomly spread and that they aligned similarly. JET results can thus be interpreted in the light of this previous analysis and we can argue that beryllium is more tensile stressed in the 2011–2012 campaign tile than in the 2013–2014 campaign tile. In particular, red points (2011–2012 campaign tile) are clearly at lower frequencies and higher widths that blue points (2013–2014 campaign tile), and they compare well with stressed beryllium carbide points measured in [18].

Fig. 5 displays the Raman spectrum of a laboratory sample that was synthetized by codepositing Be,O and C in a D_2 atmosphere, to mimicking the composition of deposits found on JET divertor tile 1. A photoluminescence background, with an origin that has to be

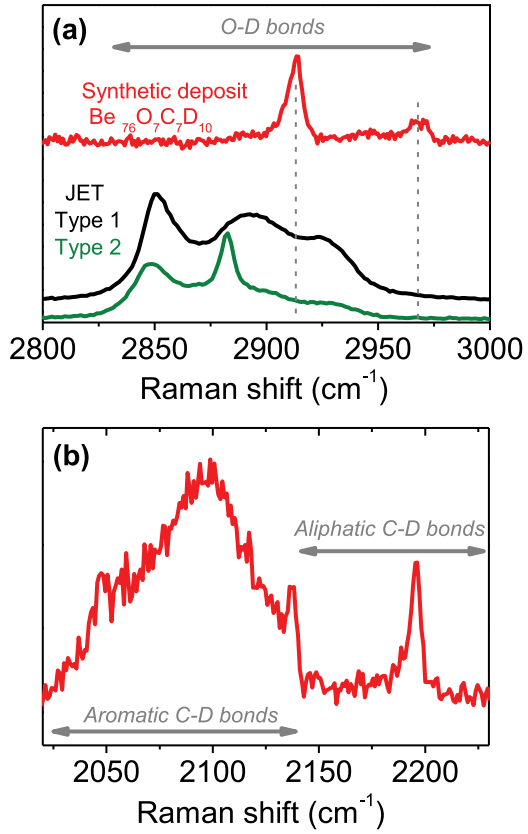

Fig. 5. Comparison of a sample mimicking JET tile 1 divertor deposit (non-melted) and the 2011–2012 campaign tile (melted). (a) O—D spectral region. (b) C—D spectral region. Note that a very intense background, not yet understood, has been subtracted from the synthetic deposit spectrum.

understood, has been subtracted. Bands are found at 2047, 2098, 2137, 2196, 2913 and 2968 cm^{-1}. They are due to aromatic C—D bonds for the 2047, 2098 and 2137 cm^{-1} bands, aliphatic C-D bonds for the 2196 cm^{-1} band and Be—O—D bonds for the 2913 and 2968 cm^{-1} bands. This last band may also be due to D_2 trapped in vacancies, but it needs more investigations [15]. D was then found to be bond with both O and C but we did not detect Be—D bonds.

4. Discussion

Deuteroxides are found by detecting Be—O and O—D vibrational modes in melted zones of 2011–2012 campaign JET tile. These modes are detected neither in non-melted zones of the 2011–2012 campaign tile nor in the 2013–2014 campaign tile. We have identified three types of deuteroxides that seem approximately concentrically organized around a ≈ 10 μm nucleus containing BeO. Type 3 is found only mixed with BeO in the nucleus while Type 2 is found at its surrounding and Type 1, which actually covers the largest area in Fig. 3d, is found in between Type 2 and a tensile stressed Be phase. We have observed that the couple of bands at 1295 and 2882 cm^{-1} is representative of Type 1 whereas the couple of bands at 1437 and 2848 cm^{-1} is representative of Type 2. In [32] deuteroxides were obtained by laser ablating a beryllium target in deuterated water and collecting the molecules formed in a cryogenic matrix and three molecules were obtained: D—⊖ Be—O—Be—D, Be(OD)2 and D—Be—OD. According to band frequencies collected in [30], our Type 1 phase may be composed of D bonded mainly like in D—Be—O—Be—D and D—Be—OD whereas the Type 2 phase may be composed of D bonded mainly like in $Be(OD)_2$ bonds. Type 3 is similar to Type 1, but with the presence of BeO wurtzite nanocrystallites in its vicinity (let us recall that the lateral resolution in Raman is micrometric). D is then trapped in various physico-chemical environments. The stoichiometry of Type 1 may be estimated in the range $Be_{1\text{-}2}O_1D_2$, for Type 1 and BeO_2D_2 for Type 2. Remarkably, beryllium hydride was not detected. Note that its low Raman cross section however makes its detection difficult.

The nucleus containing BeO schematized in Fig. 4 is about 10 μm wide and TEM measurements show that it extends down to 2 μm in depth. This corresponds to a thickness much larger than that of native oxide layer found at the surface of Be samples due to air contamination. A thin layer would actually not lead to intense signal. The presence of such a nucleus probably reveals that, when melting occurs, there is a massive diffusion and concentration of the oxygen deeply trapped in the bulk of the pristine Be material which leads to the formation of beryllium oxide nuclei and also, thanks to the concomitant ion bombardment, to the formation of deuteroxides. Note that the source of oxygen contamination that leads to these oxides and hydroxides cannot be inferred to sample air exposure after being extracted from the tokamak but comes from residual vacuum and leaks. The zone analyzed in Fig. 3, for example, is ≈ 2 μm thick, far from the typical nanometer scale contamination that can occur after venting.

In both Type 1 and 2, a weak asymmetric band at 2720 cm^{-1} is recorded, which might be attributed to trapped D_2O molecules. The vibrational frequencies of trapped D_2O depend strongly on the host material because of possible strong non covalent interactions: ν_1 and ν_3 modes of D_2O trapped in inert matrices are at 2655 and 2765 cm^{-1}, respectively [33], whereas they lie in the range 2200–2679 cm^{-1} for crystalline deuterated hydrates [34]. The asymmetry of the band at 2720 cm^{-1} could thus be due the overlapping of modes ν_1 and ν_3. Trapped H_2O molecules display a broad band at about 1200 cm^{-1} [35], which, taking into account an isotopic shift, would correspond to a frequency of 870 cm^{-1} for trapped D_2O. This value is close to the weak and broad bands observed at 855 cm^{-1} in Type 2 and 878 cm^{-1} in Type 3. This analysis shows that a small amount of D_2O may be trapped together with deuteroxides.

Pletnev et al found in [36] that behoite β-$Be(OH)_2$ incompletely dehydrates when heated to 770 K, forming water and two phases: a first phase with BeO coordinated with OH groups and a second phase of amorphous oxyhydroxide, vanishing at 1470 K. In our study, the sample was melted, meaning the temperature rose above 1470 K. Our observation of the various deuteroxide types with the presence of beryllium oxide, together with the absence of the behoite phase, is thus consistent with these results from [36]. Note that the temperature at which the behoite phase decomposes is close to the 680 K thermal desorption peak of D_2 reported in [16].

The presence of tensile stress in the beryllium phase neighboring Type 1 deuteroxide is attested in Figs. 3d and 4 by the downshift of the 455 cm^{-1} Be band. There are strong similarities in the Be band frequency versus width behavior with that of reference sample of Be_2C [18] where Be neighboring Be carbide was stressed. These results then suggest that here Be is stressed by the surrounding hydroxide phase or hydrogenated amorphous carbon phase present almost everywhere, stress being induced by the volume occupied by species with CD or OD bonds.

Analyzing the 3D structure is necessary to get a deeper insight on these processes and Raman information should be crossed with the EELS (Energy Electron Loss Spectroscopy) analysis performed on a TEM (Transmission Electron Microscopy) cross section of a FIB (Focused Ion Beam) slice cut in this zone. From the absolute Raman band intensities, we cannot yet derive quantitative data because of the 3D structure of the material which affects light propagation and because the Raman cross sections for the involved compounds are not yet all available.

5. Conclusion

We have analyzed with a micrometric lateral resolution two tiles occupying the same place in the limiter upper dump plate of the JET-

ILW tokamak during the two campaigns, 2011–12 and 2013–14, using Raman mapping. In particular, we have analyzed melted zones of the 2011–12 campaign tile where we have detected the wurtzite beryllium oxide BeO phase and various species attributed to deuteroxides BeO_xD_y. Three types of deuteroxides were observed, corresponding to different stoichiometries, none of them being the well-documented crystalline phase, the behoite β-phase. This is in agreement with what is known about the thermal stability of this phase. The presence of a small amount of D_2O is also suspected. On the contrary, no oxides nor deuteroxides were detected in the non-melted 2013–2014 campaign tile. Our results therefore suggest that D trapping occurs after melting through the formation of deuteroxides. The temperature increase favors the migration of oxygen impurities which favors deuterium trapping through OD bonding. For the laboratory sample mimicking the composition of deposits found on JET divertor tile 1, D was found to bond with both O and C but we did not detect Be-D bonds. This confirms that the formation of deuteroxides is probably an efficient way of trapping D. Note that it can also affect droplet formation and composition. To check the importance of melting in these processes, we have to compare ours results with additional data, especially from deposited zones in JET. Impact on retention is not in the scope of this paper as Raman cross section of these compounds are not yet know.

Conflict of interest

The authors declare no conflict of interest.

Acknowledgements

This work has been carried out within the framework of the EUROfusion Consortium and has received funding from the Euratom research and training programme 2014–2018 under grant agreement No 633053. The views and opinions expressed herein do not necessarily reflect those of the European Commission.

Bibliography

[1] S. Brezinsek, J.W. Coenen, T. Schwarz-Selinger, K. Schmid, A. Kirschner, A. Hakola, F.L. Tabares, H.J. van der Meiden, M.L. Mayoral, M. Reinhart, E. Tsitrone, T. Ahlgren, M. Aints, M. Airila, S. Almaviva, E. Alves, T. Angot, V. Anita, R.A. Parra, F. Aumayr, M. Balden, J. Bauer, M. Ben Yaala, B.M. Berger, R. Bisson, C. Bjorkas, I.B. Radovic, D. Borodin, J. Bucalossi, J. Butikova, B. Butoi, I. Cadez, R. Caniello, L. Caneve, G. Cartry, N. Catarino, M. Cekada, G. Ciraolo, L. Ciupinski, F. Colao, Y. Corre, C. Costin, T. Craciunescu, A. Cremona, M. De Angeli, A. de Castro, R. Dejarnac, D. Dellasega, P. Dinca, T. Dittmar, C. Dobrea, P. Hansen, A. Drenik, T. Eich, S. Elgeti, D. Falie, N. Fedorczak, Y. Ferro, T. Fornal, E. Fortuna-Zalesna, L. Gao, P. Gasior, M. Gherendi, F. Ghezzi, Z. Gosar, H. Greuner, E. Grigore, C. Grisolia, M. Groth, M. Gruca, J. Grzonka, J.P. Gunn, K. Hassouni, K. Heinola, T. Hoschen, S. Huber, W. Jacob, I. Jepu, X. Jiang, I. Jogi, A. Kaiser, J. Karhunen, M. Kelemen, M. Koppen, H.R. Koslowski, A. Kreter, M. Kubkowska, M. Laan, L. Laguardia, A. Lahtinen, A. Lasa, V. Lazic, N. Lemahieu, J. Likonen, J. Linke, A. Litnovsky, C. Linsmeier, T. Loewenhoff, C. Lungu, M. Lungu, G. Maddaluno, H. Maier, T. Makkonen, A. Manhard, Y. Marandet, S. Markelj, L. Marot, C. Martin, A.B. Martin-Rojo, Y. Martynova, R. Mateus, D. Matveev, M. Mayer, G. Meisl, N. Mellet, A. Michau, J. Miettunen, S. Moller, T.W. Morgan, J. Mougenot, M. Mozetic, V. Nemanic, R. Neu, K. Nordlund, M. Oberkofler, E. Oyarzabal, M. Panjan, C. Pardanaud, P. Paris, M. Passoni, B. Pegourie, P. Pelicon, P. Petersson, K. Piip, G. Pintsuk, G.O. Pompilian, G. Popa, C. Porosnicu, G. Primc, M. Probst, J. Raisanen, M. Rasinski, S. Ratynskaia, D. Reiser, D. Ricci, M. Richou, J. Riesch, G. Riva, M. Rosinski, P. Roubin, M. Rubel, C. Ruset, E. Safi, G. Sergienko, Z. Siketic, A. Sima, B. Spilker, R. Stadlmayr, I. Steudel, P. Strom, T. Tadic, D. Tafalla, I. Tale, D. Terentyev, A. Terra, V. Tiron, I. Tiseanu, P. Tolias, D. Tskhakaya, A. Uccello, B. Unterberg, I. Uytdenhoven, E. Vassallo, P. Vavpetic, P. Veis, I.L. Velicu, J.W.M. Vernimmen, A. Voitkans, U. von Toussaint, A. Weckmann, M. Wirtz, A. Zaloznik, R. Zaplotnik, W.P. Contributors, Plasma-wall interaction studies within the EUROfusion consortium: progress on plasma-facing components development and qualification, Nucl. Fusion 57 (2017).

[2] G.F. Matthews, M. Beurskens, S. Brezinsek, M. Groth, E. Joffrin, A. Loving, M. Kear, M.L. Mayoral, R. Neu, P. Prior, V. Riccardo, F. Rimini, M. Rubel, G. Sips, E. Villedieu, P. de Vries, M.L. Watkins, E.-J. Contributors, JET ITER-like wall-overview and experimental programme, Phys. Scr. T145 (2011).

[3] M. Mayer, S. Krat, A. Baron-Wiechec, Y. Gasparyan, K. Heinola, S. Koivuranta, J. Likonen, C. Ruset, G. de Saint-Aubin, A. Widdowson, J.E.T. Contributors, Erosion and deposition in the JET divertor during the second ITER-like wall campaign, Phys. Scr. T170 (2017).

[4] R. Neu, A.U. Team, E.P. Taskforce, J.E. Contributors, Preparing the scientific basis for an all metal ITER, Plasma Phys. Control. Fusion 53 (2011).

[5] S. Brezinsek, A. Widdowson, M. Mayer, V. Philipps, P. Baron-Wiechec, J.W. Coenen, K. Heinola, A. Huber, J. Likonen, P. Petersson, M. Rubel, M.F. Stamp, D. Borodin, J.P. Coad, A.G. Carrasco, A. Kirschner, S. Krat, K. Krieger, B. Lipschultz, C. Linsmeier, G.F. Matthews, K. Schmid, J.E.T. Contributors, Beryllium migration in JET ITER-like wall plasmas, Nucl. Fusion 55 (2015).

[6] I. Bykov, H. Bergsaker, G. Possnert, Y. Zhou, K. Heinola, J. Pettersson, S. Conroy, J. Likonen, P. Petersson, A. Widdowson, J.E.T. Contributors, Studies of Be migration in the JET tokamak using AMS with Be-10 marker, Nucl. Instrum. Methods Phys. Res. Sect. B-Beam Interact. Mater. Atoms 371 (2016) 370–375.

[7] K. Krieger, S. Brezinsek, M. Reinelt, S.W. Lisgo, J.W. Coenen, S. Jachmich, S. Marsen, A. Meigs, G. van Rooij, M. Stamp, O. van Hoey, D. Ivanova, T. Loarer, V. PhilippsJ.E.T.E.F.D.A. Contributors, Beryllium migration and evolution of first wall surface composition in the JET ILW configuration, J. Nucl. Mater. 438 (2013) S262–S266.

[8] K. Schmid, M. Reinelt, K. Krieger, An integrated model of impurity migration and wall composition dynamics for tokamaks, J. Nucl. Mater. 415 (2011) S284–S288.

[9] E. Fortuna-Zalesna, J. Grzonka, S. Moon, M. Rubel, P. Petersson, A. Widdowson, J.E.T. Contributors, Fine metal dust particles on the wall probes from JET-ILW, Phys. Scr. T170 (2017).

[10] E. Fortuna-Zalesna, J. Grzonka, M. Rubel, A. Garcia-Carrasco, A. Widdowson, A. Baron-Wiechec, L. Ciupinski, J.E.T. Contributors, Studies of dust from JET with the ITER-Like Wall: Composition and internal structure, Nucl. Mater. Energy 12 (2017) 582–587.

[11] S. Masuzakil, M. Tokitanii, T. Otsuka, Y. Oya, Y. Hatan, M. Miyamoto, R. Sakamoto, N. Ashikawa, S. Sakurada, Y. Uemura, K. Azuma, K. Yumizurus, M. Oyaizu, T. Suzuki, H. Kurotaki, D. Hamaguchi, K. Isobel, N. Asakura, A. Widdowson, K. Heinola, S. Jachmich, M. Rubel, J.E.T. contributors, Analyses of microstructure, composition and retention of hydrogen isotopes in divertor tiles of JET with the ITER-like wall, Phys. Scr. T170 (2017).

[12] K. Heinola, A. Widdowson, J. Likonen, E. Alves, A. Baron-Wiechec, N. Barradas, S. Brezinsek, N. Catarino, P. Coad, S. Koivuranta, Long-term fuel retention in JET ITER-like wall, Phys. Scr. T167 (2016) 014075.

[13] J. Likonen, K. Heinola, A. De Backer, S. Koivuranta, A. Hakola, C.F. Ayres, A. Baron-Wiechec, P. Coad, G.F. Matthews, M. Mayer, A. Widdowson, J. Contributors, Deuterium trapping and release in JET ITER-like wall divertor tiles, Phys. Scr. T167 (2016) 014074.

[14] E.A. Hodille, F. Ghiorghiu, Y. Addab, A. Zaloznik, M. Minissale, Z. Piazza, C. Martin, T. Angot, L. Gallais, M.F. Barthe, C.S. Becquart, S. Markelj, J. Mougenot, C. Grisolia, R. Bisson, Retention and release of hydrogen isotopes in tungsten plasma-facing components: the role of grain boundaries and the native oxide layer from a joint experiment-simulation integrated approach, Nucl. Fusion 57 (2017).

[15] E.A. Hodille, Y. Ferro, Z.A. Piazza, C. Pardanaud, Hydrogen in beryllium oxide investigated by DFT: on the relative stability of charged-state atomic versus molecular hydrogen, J. Phys. Condens. Matter 30 (2018).

[16] M. Reinelt, C. Linsmeier, Ion implanted deuterium retention and release from clean and oxidized beryllium, J. Nucl. Mater. (2009) 568–571 390-91.

[17] C. pardanaud, C. Martin, P. Roubin, Raman Microscopy: A Suitable Tool for Characterizing Surfaces in Interaction with Plasmas in the Field of Nuclear Fusion, in: K Maaz (Ed.), Raman Spectroscopy and Applications, InTech, 2017, pp. 3–30.

[18] M.I. Rusu, C. Pardanaud, Y. Ferro, G. Giacometti, C. Martin, Y. Addab, P. Roubin, M. Minissale, L. Ferri, F. Virot, M. Barrachin, C.P. Lungu, C. Porosnicu, P. Dinca, M. Lungu, M. Koppen, P. Hansen, C. Linsmeier, Preparing the future post-mortem analysis of beryllium-based JET and ITER samples by multi-wavelengths Raman spectroscopy on implanted Be, and co-deposited Be, Nucl. Fusion (2017) 57.

[19] C. Pardanaud, M.I. Rusu, G. Giacometti, C. Martin, Y. Addab, P. Roubin, C.P. Lungu, C. Porosnicu, I. Jepu, P. Dinca, M. Lungu, O.G. Pompilian, R. Mateus, E. Alves, M. Rubel, J. contributors, Raman microscopy investigation of beryllium materials, Phys. Scr. T167 (2016) 014027.

[20] C. Pardanaud, M.I. Rusu, C. Martin, G. Giacometti, P. Roubin, Y. Ferro, A. Allouche, M. Oberkofler, M. Köppen, T. Dittmar, C. Linsmeier, Hydrogen retention in beryllium: concentration effe ocrystalline growth, J. Phys. Condens. Matter 27 (2015) 475401.

[21] K. Heinola, A. Widdowson, J. Likonen, T. Ahlgren, E. Alves, C.F. Ayres, A. Baron-Wiechec, N. Barradas, S. Brezinsek, N. Catarino, P. Coad, C. Guillemaut, I. Jepu, S. Krat, A. Lahtinen, G.F. Matthews, M. Mayer, J.E.T. Contributors, Experience on divertor fuel retention after two ITER-Like Wall campaigns, Phys. Scr. T170 (2017).

[22] C.P. Lungu, C. Porosnicu, I. Jepu, M. Lungu, A. Marcu, C. Luculescu, C. Ticos, A. Marin, C.E.A. Grigorescu, The behavior of W, Be and C layers in interaction with plasma produced by terawatt laser beam pulses, Vacuum 110 (2014) 207–212.

[23] A. Hakola, K. Heinola, J. Likonen, C. Lungu, C. Porosnicu, E. Alves, R. Mateus, I. Bogdanovic Radovic, Z. Siketic, V. Nemanic, C. Pardanaud, a.E.W.P. Contributors, Production of JET-ILW relevant Be-containing laboratory samples for fuel retention investigations, Nucl. Mater. Energy (2018) This volume.

[24] X.Y. An, T.X. Zeng, W.Y. Ren, Structural, electronic and optical properties of BeH2: A density functional theory study, Mater. Res. Express 4 (2017).

[25] C. Pépin, P. Loubeyre, Layered structure and re-entrant disproportionation observed in crystalline BeH2 under pressure, Phys. Rev. B 93 (2016) 224104.

[26] U.D. Wdowik, Structural stability and thermal properties of BeO from the quasi-harmonic approximation, J. Phys.Condens. Matter 22 (2010).

[27] F. Luo, Z.C. Guo, X.L. Zhang, C.Y. Yuan, C.A. Liu, L.C. Cai, Pressure effects on structural and elastic properties of BeO from first-principles calculations, Phys. Status Solidi B-Basic Solid State Phys. 252 (2015) 212–218.

[28] A. Bosak, K. Schmalzl, M. Krisch, W. van Beek, V. Kolobanov, Lattice dynamics of

beryllium oxide: inelastic x-ray scattering and ab initio calculations, Phys. Rev. B 77 (2008).
[29] S.T. Zhang, F. Li, H.Y. Xu, G.C. Yang, Pressure-induced stable beryllium peroxide, Inorg. Chem. 56 (2017) 5233–5238.
[30] C. Pardanaud, C. Martin, P. Roubin, G. Giacometti, C. Hopf, T. Schwarz-Selinger, W. Jacob, Raman spectroscopy investigation of the H content of heated hard amorphous carbon layers, Diam. Relat. Mater. 34 (2013) 100–104.
[31] H.D. Lutz, C. Jung, R. Mortel, H. Jacobs, R. Stahl, Hydrogen bonding in solid hydroxides with strongly polarising metal ions, beta-Be(OH)(2) and epsilon-Zn(OH)(2), Spectrochim. Acta Part a-Mol. Biomol. Spectrosc. 54 (1998) 893–901.
[32] C.A. Thompson, L. Andrews, Reactions of laser ablated be atoms with H2O: Infrared spectra and density functional calculations of HOBeOH, HBeOH, and HBeOBeH, J. Phys. Chem. 100 (1996) 12214–12221.
[33] S. Coussan, P. Roubin, J.P. Perchard, Infrared induced isomerizations of water polymers trapped in nitrogen matrix, Chem. Phys. 324 (2006) 527–540.
[34] W. Mikenda, S. Steinbock, Stretching frequency versus bond distance correlation of O-D(H)...F hydrogen-bonds in solid hydrates, J. Mol. Struct. 326 (1994) 123–130.
[35] W.W. Rudolph, D. Fischer, G. Irmer, C.C. Pye, Hydration of beryllium(II) in aqueous solutions of common inorganic salts. a combined vibrational spectroscopic and ab initio molecular orbital study, Dalton Trans. (2009) 6513–6527.
[36] R.N. Pletnev, V.S. Kiiko, Y.N. Makurin, A.A. Nepryakhin, Proton magnetic resonance and the state of hydrogen in beryllium hydroxide, Refract. Ind. Ceram. 46 (2005) 273–275.